Prostate Boundary Segment Extraction using Cascaded Shape Regression and Optimal Surface Detection

Jierong Cheng[1], Wei Xiong[1], Ying Gu[1], Shue Ching Chia[1], Yue Wang[1], Weimin Huang[1], Jiayin Zhou[1], Yufeng Zhou[2], Wilson Gao[2], Kae Jack Tay[3] and Henry Ho[3]

***Abstract*— In this paper, we proposed a new method (CSR+OSD) for the extraction of irregular open prostate boundaries in noisy extracorporeal ultrasound image. First, cascaded shape regression (CSR) is used to locate the position of prostate boundary in the images. In CSR, a sequence of random fern predictors are trained in a boosted regression manner, using shape-indexed features to achieve invariance against position variations of prostate boundaries. Afterwards, we adopt optimal surface detection (OSD) to refine the prostate boundary segments across 3D sections globally and efficiently. The proposed method is tested on 162 ECUS images acquired from 8 patients with benign prostate hyperplasia. The method yields a Root Mean Square Distance of 2.11±1.72 mm and a Mean Absolute Distance of 1.61±1.26 mm, which are lower than those of JFilament, an open active contour algorithm and Chan-Vese region based level set model, respectively.**

I. Introduction

High Intensity Focused Ultrasound (HIFU) is being used throughout the world as a therapeutic procedure for prostate cancer and benign prostate hyperplasia (BPH). An important component in BPH removal using HIFU is to position and focus on the targeted prostate tissue which is obstructing the urethra. The boundary segment between the prostate and the bladder is particularly important in ultrasound image guided BPH tissue removal. Automatic prostate boundary extraction from ECUS images faces considerable challenges. First, extracorporeal ultrasound (ECUS) images are usually noisier than transrectal ultrasound (TRUS) images. Second, the above mentioned prostate boundary segment is an irregular open contour. Last, the prostate boundary is of large variation between patients with BPH which makes shape modeling extremely difficult.

Numerous prostate segmentation methods have been developed in literature, either for TRUS, MR, or CT images (see [1] for an extensive review). However, existing work on prostate segmentation in ECUS images is very rare and none of the methods were tested on ultrasound images of prostate with BPH. In [1], the prostate segmentation methods are classified into four groups according to the information used to guide the segmentation: contour and shape based method, region based methods, supervised and un-supervised classification methods, and hybrid methods. The first group of methods, e.g. active contour model [2] and curve fitting [3], [4] alone are often ineffective because of the unreliable and even broken edges in ECUS images. Active shape model and active appearance model based methods [5], [6] need good initialization since they are local optimization. Region based methods such as graph partitioning [7] and regional level set [8], solve the segmentation problem in an energy minimization framework. However, region based methods are not directly applicable when the targeted boundary is an open contour, and neither are the classification methods which cluster or classify the pixels into the prostate or the background based on feature vectors.

In this paper, we propose a new method (CSR+OSD) for the extraction of the prostate boundary segments with BPH in ECUS images. The cascaded shape regression (CSR) method [9] is able to efficiently locate the prostate boundary against position variations, given a set of training data. Following CSR, the optimal surface detection (OSD) method [10] is adopted to optimize the detected boundaries in a sequence of ultrasound images simultaneously.

II. Cascaded Shape Regression

In the CSR method, a prostate boundary is represented by a sequence of M landmark points: $S = [x_1, y_1, ..., x_M, y_M]^T$. As a landmark-based shape model, an essential requirement is that landmarks on all training samples are located at corresponding positions. To find these landmarks, equally-distanced landmarks are selected automatically from the manually drawn prostate boundary. Each training sample, $\{(I_i, \hat{S}_i)\}$, consists of an image I_i and a true boundary $\hat{S}_i$, $i = 1, 2, ..., N$.

A cascaded regressor $R = (R^1, R^2, ..., R^T)$ consists of T weak regressors. Given an image I and an initial prostate boundary S^0, each regressor generates a boundary increment vector δS to update the previous boundary and the output of regressors R^t depends on image I and the previous boundary S^{t-1}:

$$S^t = S^{t-1} + \delta S^t,$$
$$\text{with } \delta S^t = R^t(I, S^{t-1}), t = 1, 2, ..., T. \quad (1)$$

Each regressor is trained to minimize the difference between the true boundary and the new boundary updated by the regressor, i.e.,

$$R^t = \arg\min_R \sum_{i=1}^{N} \|\hat{S}_i - (S_i^{t-1} + R(I_i, S_i^{t-1})\|_2. \quad (2)$$

We use random ferns [11] as weak regressors in the cascade. A fern regressor is created by randomly selecting

[1]Institute for Infocomm Research, 1 Fusionopolis Way, Singapore 138632
[2]School of Mechanical and Aerospace Engineering, Nanyang Technological University, 50 Nanyang Avenue, Singapore 639798
[3]Department of Urology, Singapore General Hospital, Outram Road, Singapore 169608

978-1-4244-7929-0/14/$26.00 ©2014 IEEE

s features from a vector of F features and comparing them with s thresholds randomly selected. In this way, each input feature vector is divided into one of 2^s bins. Each bin b is associated with a regression output δS_b that minimizes the alignment error of training samples Ω_b that fall into the bin:

$$\delta S_b = \arg\min_{\delta S} \sum_{i \in \Omega_b} \|\hat{S}_i - (S_i + \delta S)\|_2. \quad (3)$$

Eqn. (3) is solved by simply taking the mean of all boundary differences. At each stage in the cascaded regression, a pool of K ferns are randomly generated and the one with the lowest regression error is chosen.

A. Shape-indexed Features

Given a set of training data, we used simple shape-indexed features to learn each regressor. Shape-indexed features mean that a pixel is indexed relative to the currently estimated boundary rather than the original image coordinates. These features are computed as the intensity difference between two pixels in the image. In [9], the prostate shape was fitted to an ellipse to reflect the translation, scale, and rotation of the shape. However, this method cannot be applied to the extraction of an irregular open boundary of prostate.

To compute one shape-indexed feature from the current estimated boundary, we randomly sample two pixels, (dx_1, dy_1) and (dx_2, dy_2), within a circle of radius r centered at $(0, 0)$ and one random integer $n \in [1, M]$. The intensity difference at the two pixels, $p_1 = (x_n + dx_1, y_n + dy_1)$ and $p_2 = (x_n + dx_2, y_n + dy_2)$, result in a shape-indexed feature $I(p_1) - I(p_2)$. Here (x_n, y_n) are the coordinates of nth landmark points on the current boundary.

B. Training for CSR

For each training sample S_i, we use the average of all training boundaries $\left(S^0 = \frac{\sum_{j=1}^{N} \hat{S}_j}{N}\right)$ and the true boundary of the rest of training samples $\{\hat{S}_j | j = 1, 2, ..., N, j \neq i\}$ to initialize the CSR. The CSR is trained to move the boundary to the true boundary $\hat{S}_i$ even if the initial positions are far from $\hat{S}_i$. For each testing sample, CSR is only initialized for once by the average boundary because it is the single boundary estimate that minimize the training error before regression starts. The training process for CSR is summarized in Algorithm 1.

Initialize $S_i^0, i = 1, 2, ..., N$;
for $t = 1$ *to* T **do**
  for $i = 1$ *to* N **do**
    Compute shape-indexed features;
  end
  Train K random ferns on all N current boundaries;
  Select the best fern which gives the lowest training error;
  Compute $\delta S_b = R_b^t$ for each bin b in the best fern;
  for $i = 1$ *to* N **do**
    $S_i^t = S_i^{t-1} + \delta S_b$, suppose the features of S_i^{t-1} fall into bin $b, b \in \{1, 2, ..., 2^s\}$;
  end
end
Return $R = (R^1, R^2, ..., R^T)$;

Algorithm 1: Training for cascaded shape regression

III. Optimal Surface Detection

Given the CSR result as an estimation of the prostate boundary, we adopted the optimal surface detection (OSD) method [10] to refine the prostate boundary segments across 3D sections globally and efficiently. The method transformed the surface segmentation problem into computing a minimum s-t cut in a derived arc-weighted directed graph. An optimal surface controlled by the cost function and geometric constraints is found in a polynomial time.

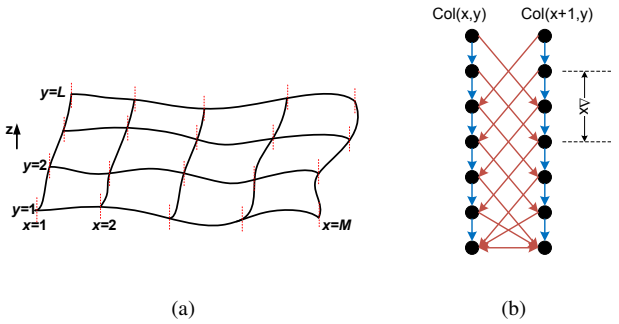

Fig. 1. (a) Overall graph structure used in OSD. Dotted vertical lines (in red) are *columns*. (b) Detailed structure in two adjacent columns: blue vertical arrows for intra-column arcs and red slant arrows for inter-column arcs.

A. Graph construction

Suppose a sequence of ECUS images consists of L frames, each containing a 2D prostate contour resulted from CSR with M landmark points. A terrain-like surface is defined by a function $\mathcal{N}$: $(x, y) \rightarrow \mathcal{N}(x, y)$, where $x \in \mathbf{x} = \{1, 2, ..., M\}$, $y \in \mathbf{y} = \{1, 2, ..., L\}$, and $\mathcal{N}(x, y) \in \mathbf{z} = \{1, 2, ..., Z\}$. Z is the number of voxels on a *column* along the normals of the surface.

A node-weighted graph $G = (V, E)$ is constructed according to $\mathcal{I}$, where each node $V(x, y, z) \in V$ represents exactly one voxel at $(x, y, z) \in \mathcal{I}$. Intra-column arcs connect nodes of a same column $Col(x, y)$ from $V(x, y, z)$ $(z > 1)$ to $V(x, y, z - 1)$, i.e.,

$$E^a = \{\langle V(\mathbf{x}, \mathbf{y}, z), V(\mathbf{x}, \mathbf{y}, z - 1)\rangle | z > 1\}. \quad (4)$$

Inter-column arcs connect nodes of adjacent columns, i.e.

$$E^r = \begin{cases} \{\langle V(x, \mathbf{y}, z), V(x \pm 1, \mathbf{y}, \max(1, z - \Delta_x)\rangle\} \\ \{\langle V(\mathbf{x}, y, z), V(\mathbf{x}, y \pm 1, \max(1, z - \Delta_y)\rangle\}, \end{cases} \quad (5)$$

where Δ_x and Δ_y are smoothness parameters controlling surface connectivity. Each arc in $E = \{E^a \cup E^r\}$ is assigned an infinity cost.

B. Cost function

A cost value $c(x, y, z)$ is computed for each voxel at (x, y, z) of $\mathcal{I}$. $c(x, y, z)$ is inversely related to the likelihood that $\mathcal{I}(x, y, z)$ belongs to the desired surface. A weight $w(x, y, z)$ is then assigned to each node $V(x, y, z)$:

$$w(x,y,z) = \begin{cases} c(x,y,z), & \text{if } z = 1, \\ c(x,y,z) - c(x,y,z-1), & \text{otherwise.} \end{cases} \tag{6}$$

To construct an arc-weighted directed graph, two special nodes, the *source* s and the *sink* t, are added. Additional directed arcs are created from s to nodes with $w(x, y, z) < 0$ and from nodes with $w(x, y, z) \geq 0$ to t. These arcs are of cost $|w(x, y, z)|$.

An approximation of Chan-Vese cost functional [12] was proposed to be used in voxel cost computation in [10]. Specifically, the voxel cost is assigned as the

$$c(x,y,z) = \sum_{z' \leq z} (\mathcal{I}(x,y,z') - a_1)^2 + \sum_{z' > z} (\mathcal{I}(x,y,z') - a_2)^2, \tag{7}$$

where a_1 and a_2 are the mean intensities in the interior and exterior of the surface. They can be approximated by

$$\hat{a}_1(x,y,z) = \text{mean}(\mathcal{I}(\mathbf{x}', \mathbf{y}', \mathbf{z}'_1)), \tag{8}$$

$$\hat{a}_2(x,y,z) = \text{mean}(\mathcal{I}(\mathbf{x}', \mathbf{y}', \mathbf{z}'_2)), \tag{9}$$

where $\mathbf{z}'_1 \equiv \{z' | z' \leq \max(1, z - |x' - x|\Delta_x - |y' - y|\Delta_y)\}$ and $\mathbf{z}'_2 \equiv \{z' | z + |x' - x|\Delta_x + |y' - y|\Delta_y) < z' \leq Z\}$.

In ECUS images, the interior of the surface (prostate) appears to be brighter than the exterior of the surface (bladder), i.e. $\hat{a}_1 > \hat{a}_2$. We propose a modified cost function to make use of this condition:

$$c'(x,y,z) = \begin{cases} c(x,y,z), & \text{if } \hat{a}_1 > \hat{a}_2, \\ c(x,y,z) + 100(\hat{a}_1 - \hat{a}_2)^2, & \text{otherwise,} \end{cases} \tag{10}$$

so that edges with $\hat{a}_1 < \hat{a}_2$ are penalized with higher cost.

Once the graph is constructed and the cost function is defined, the optimal surface that intersects one node of each column and minimizes globally the cost function is computed with an s-t cut algorithm [13].

IV. Results

We validate the performance of our method (CSR+OSD) on a total of 162 ECUS images acquired from 8 patients with BPH. From each patient, a sequence of prostate images is acquired by a motor controlled ultrasound transducer at a constant rotation angle of one degree per 6-7 frames. The resolution of the images is 800×600 pixels (0.354 mm/pixel). The ground truth (true boundaries) are manually drawn and each prostate boundary is described by $M = 20$ landmarks. The parameters of the CSR are set as follows: number of training data $N = 50$, number of phases in the cascade $T = 390$, fern depth $s = 5$, number of ferns $K = 32$, radius $r = 300$, and number of features $F = 100$. To avoid bias in such a splitting in the experiment, five-fold cross validation (4 for training and 1 for testing) is adopted. We set the parameters in OSD as follows: $\Delta_x = 5$, $\Delta_y = 8$, the sampling step along columns $\delta = 1$, and the sampling range is 30 pixels. Our method is implemented in C on a PC with 2.83GHz CPU and 8GB RAM. The training and testing time of CSR are 23 minute for 32 images and 0.03 seconds per image, respectively. The computational time of OSD is 3.3 seconds per image.

We use average Root Mean Square Distance (RMSD) and Mean Absolute Distance (MAD) to evaluate the segmentation result. The results are compared with those from JFilament [14] and Chan-Vese region-based level set model [12]. JFilament is a software tool based on stretching open active contours or "snakes" [15], developed for segmentation and tracking of 2D and 3D filaments in fluorescenece microscopy images. The parameters in JFilament are set to: Alpha = 0, Beta = 0, Gamma = 400, Weight = 1, Stretch Force = 100, and Deform Iterations = 200. The parameters in Chan-Vese model are set to: $\mu = 0.01 * 255^2$, $\lambda_1 = \lambda_2 = 1$, $\nu = 0$, and the number of iterations is 30. When computing RMSD and MAD, the corresponding points to each landmarks on the true boundary are those closest points in the results of JFilament/Chan-Vese model. The prostate boundary segments detected by different methods are compared in Fig. 2.

For the snake based JFilament, we initialize it by the average of all true boundaries from the same patient/sequence. Due to the lack of strong gradient nearby the snake, JFilament tends to shrink and fail to capture prostate boundaries of high curvature. Chan-Vese model is initialized by a circle manually drawn inside the bladder on each sequence. As a region based level set method, Chan-Vese model is less sensitive to initialization and more robust to the noise in the images. Its RMSD and MAD are slightly lower than CSR+OSD in sequences where the intensities in the bladder are constantly lower than the intensities in the prostate (patient 2, 6, and 7). However, when region homogeneity is violated, Chan-Vese model generates fragmented regions and fails to capture the prostate boundary (patient 3 and 5). During the testing of CSR+OSD, we use the average of all training boundaries S^0 (which come from all the patients) as the initialization for the testing images. Although the initialization of CSR+OSD is much worse than those of JFilament and Chan-Vese model, CSR+OSD still outperforms them notably in term of overall performance (see Table I).

V. Conclusions

A novel approach has been proposed for the extraction of prostate boundary segments with BPH in ECUS images. By using CSR with shape-indexed feature, our approach is able to efficiently locate the prostate boundary against position variations in ECUS images. With the help of OSD, efficient and accurate segmentation is achieved.

ACKNOWLEDGMENT

The work is partially supported by SERC Grant No. 1211480001, A*STAR, Singapore.

TABLE I

SEGMENTATION ACCURACY (IN MM).

		JFilament		Chan-Vese		CSR		CSR+OSD	
Patient	Samples	RMSD	MAD	RMSD	MAD	RMSD	MAD	RMSD	MAD
1	17	3.78	3.08	2.81	2.08	2.66	2.13	1.60	1.24
2	13	2.20	1.85	1.29	1.08	1.49	1.19	1.34	1.17
3	26	2.33	1.98	14.22	8.81	2.12	1.65	1.70	1.26
4	28	5.83	4.83	1.99	1.45	2.72	2.12	1.86	1.37
5	11	2.74	2.16	8.20	6.25	2.67	2.09	2.04	1.61
6	23	4.82	3.78	2.75	2.02	5.11	3.85	4.43	3.30
7	20	3.10	2.66	1.22	0.93	2.11	1.61	1.31	1.05
8	24	4.74	3.89	3.04	2.44	2.90	2.26	2.12	1.62
Total	162	3.91±2.19	3.21±1.94	4.57±4.82	3.16±3.11	2.81±1.88	2.17±1.40	2.11±1.72	1.61±1.26

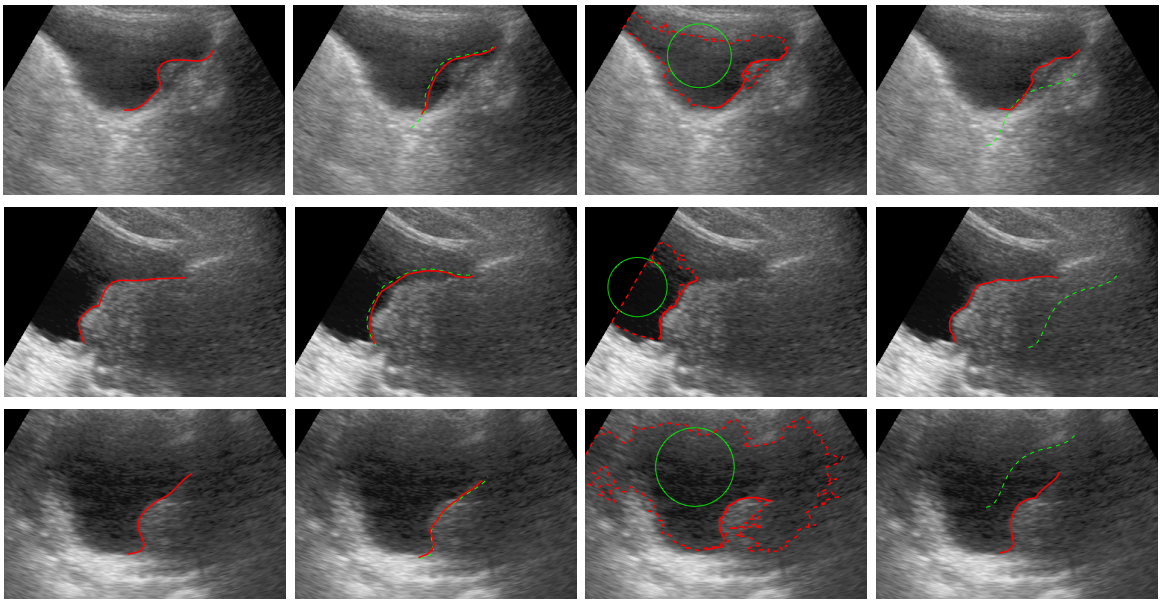

Fig. 2. Prostate boundary extraction results shown in red solid line. First column: ground truth. Second column: JFilament initialized by green dashed line. Third column: Chan-Vese model initialized by green circle. Fourth column: CSR+OSD initialized by green dashed line.

REFERENCES

[1] S. Ghose, A. Oliver, R. Mart, X. Llad, J. C. Vilanova, J. Freixenet, J. Mitra, D. Sidib, and F. Meriaudeau, "A survey of prostate segmentation methodologies in ultrasound, magnetic resonance and computed tomography images," *Computer Methods and Programs in Biomedicine*, vol. 108, no. 1, pp. 262–287, 2012.

[2] A. Zaim and J. Jankun, "An energy-based segmentation of prostate from ultrasound images using dot-pattern select cells," in *ICASSP*, 2007, pp. 297–300.

[3] L. Gong, S. D. Pathak, D. R. Haynor, P. S. Cho, and Y. Kim, "Parametric shape modeling using deformable superellipses for prostate segmentation," *IEEE Trans. Med. Imag.*, vol. 23, no. 3, pp. 340–349, 2004.

[4] S. Badiei, S. E. Salcudean, J. Varah, and W. J. Morris, "Prostate segmentation in 2D ultrasound images using image warping and ellipse fitting," in *MICCAI*, ser. LNCS, vol. 4191, 2006, pp. 17–24.

[5] P. Yan, S. Xu, B. Turkbey, and J. Kruecker, "Discrete deformable model guided by partial active shape model for TRUS image segmentation," *IEEE Trans. Biomed. Eng.*, vol. 57, no. 5, pp. 1158–1166, 2010.

[6] S. Ghose, A. Oliver, J. Mitra, R. Marti, X. Llad, J. Freixenet, D. Sidib, J. C. Vilanova, J. Comet, and F. Meriaudeau, "A supervised learning framework of statistical shape and probability priors for automatic prostate segmentation in ultrasound images," *Medical Image Analysis*, vol. 17, no. 6, pp. 587–600, 2013.

[7] M. Zouqi and J. Samarabandu, "Prostate segmentation from 2D ultrasound images using graph cuts and domain knowledge," in *Computer and Robot Vision*, 2008, pp. 359–362.

[8] F. Shao, K. V. Ling, and W. S. Ng, "3D prostate surface detection from ultrasound images based on level set method," in *MICCAI*, ser. LNCS, vol. 2489, 2002, pp. 389–396.

[9] J. Cheng, W. Xiong, Y. Gu, S.-C. Chia, and Y. Wang, "Cascaded shape regression for automatic prostate segmentation from extracorporeal ultrasound images." in *AE-CAI*, ser. LNCS, vol. 8090, 2013, pp. 65–74.

[10] K. Li, X. Wu, D. Z. Chen, and M. Sonka, "Optimal surface segmentation in volumetric images - a graph-theoretic approach," *IEEE Trans. Pattern Anal. Mach. Intell.*, vol. 28, no. 1, pp. 119–134, 2006.

[11] M. Ozuysal, M. Calonder, V. Lepetit, and P. Fua, "Fast keypoint recognition using random ferns," *IEEE Trans. Pattern Anal. Mach. Intell.*, vol. 32, no. 3, pp. 448–461, 2010.

[12] T. F. Chan and L. A. Vese, "Active contours without edges," *IEEE Trans. Image Process.*, vol. 10, no. 2, pp. 266–277, 2001.

[13] Y. Boykov and V. Kolmogorov, "An experimental comparison of Min-cut/Max-flow algorithms for energy minimization in vision," *IEEE Trans. Pattern Anal. Mach. Intell.*, vol. 26, no. 9, pp. 1124–1137, 2004.

[14] M. B. Smith, H. Li, T. Shen, X. Huang, E. Yusuf, and D. Vavylonis, "Segmentation and tracking of cytoskeletal filaments using open active contours," *Cytoskeleton*, vol. 67, no. 11, pp. 693–705, 2010.

[15] H. Li, T. Shen, M. Smith, I. Fujiwara, D. Vavylonis, and X. Huang, "Automated actin filament segmentation, tracking and tip elongation measurements based on open active contour models," in *ISBI*. IEEE, 2009, pp. 1302–1305.